Acta Geotechnica
https://doi.org/10.1007/s11440-025-02797-3

RESEARCH PAPER

The variation of large strain viscous rate effects from undrained triaxial element testing of Kaolin clay

Scott Robinson[1] · Michael J. Brown[1] · Jonathan Knappett[1] · Andrew Brennan[1] · Diego Duran Caballero[2] · Marcos Arroyo[2,3]

Received: 26 March 2025 / Accepted: 1 October 2025

Abstract

Viscous (undrained) rate effects lead to an increase in the shear strength of fine-grained soils such as clays when sheared at high strain rates. Correct rate effect parameters are key to accurate predictions of behaviour in a range of geotechnical applications, from subsea cable ploughing and rapid load testing of piles through to numerical modelling of offshore foundation systems. The factors influencing the magnitude of rate effects are, however, still poorly understood. Through a series of 100-mm diameter high-speed undrained triaxial tests (strain rates ranging from 300 to 180,000%/hr and initial effective stresses from 300 to 1350 kPa) on Kaolin clay, this paper investigates the influence of the soil state and stress history on rate effects across a wide strain range. Viscous rate effects ranging from 10 to 16% per log cycle are observed, and the liquidity index is observed to correlate to the magnitude of the rate effects. Viscous rate effects are also shown to reduce with increasing strain level, and a model is proposed which allows the rate effect in Kaolin to be predicted accounting for both of these factors. This model is potentially useful in analytical and numerical studies.

Keywords Clay · Liquidity index · Strain level · Strain-rate · Triaxial testing · Viscous rate effects

Abbreviations

A	Activity
BS	British Standard
$c_{\alpha e}$	Creep coefficient
c_u	Undrained shear strength
$c_{u,ref}$	Undrained shear strength at the reference strain rate
c_v	Coefficient of consolidation
CF	Clay Fraction
d	Characteristic length related to drainage path
k	Permeability
LI	Liquidity Index
LL	Liquid Limit
M	Gradient of CSL in q-p' space
N	Intercept on the normal consolidation line at 1 kPa
OCR	Overconsolidation Ratio
PI	Plasticity Index
PL	Plastic Limit
PPT	Pore pressure transducer
p'_{max}	Maximum mean effective stress used for over-consolidating the sample
p'_0	Mean effective stress
q	Deviator stress
q_{peak}	Maximum or peak deviator stress
$q_{peak,ref}$	Maximum or peak deviator stress at the reference strain rate
q_{ref}	Deviator stress at the reference strain rate
SSA	Specific Surface Area

✉ Scott Robinson
s.z.robinson@dundee.ac.uk

Michael J. Brown
m.j.z.brown@dundee.ac.uk

Jonathan Knappett
j.a.knappett@dundee.ac.uk

Andrew Brennan
a.j.brennan@dundee.ac.uk

Diego Duran Caballero
diego.duran.caballero@upc.edu

Marcos Arroyo
marcos.arroyo@upc.edu

[1] School of Science and Engineering, University of Dundee, Fulton Building, Dundee DD1 4HN, UK

[2] Centre Internacional de Mètodes Numèrics en Enginyeria (CIMNE), Barcelona, Spain

[3] Universitat Politècnica de Catalunya - BarcelonaTech (UPC), Barcelona, Spain

Published online: 22 October 2025

v	Axial velocity
V	Normalised velocity
α_{peak}	Material specific parameter for soil state effect (using peak strength rate effect definition)
α	Material specific parameter for soil state effect (using strain-based rate effect definition)
$\Delta\lambda_{log(\varepsilon q)}$	Reduction in rate effect per log cycle of strain
$\dot{\varepsilon}$	Axial strain rate
$\dot{\varepsilon}_{ref}$	Reference axial strain rate
ε_q	Triaxial deviatoric strain
$\dot{\varepsilon}_q$	Triaxial deviatoric strain rate
$\varepsilon_{q,EL}$	Elastic shear strain threshold
$\varepsilon_{q,\lambda max}$	Shear strain at which λ_{max} occurs
$\dot{\varepsilon}_{q,ref}$	Reference triaxial deviatoric strain rate
$\varepsilon_{q,peak}$	Shear strain at which the peak strength occurs
$\varepsilon_{q,peak,ref}$	Shear strain at which the peak strength occurs (at the reference strain rate)
κ	Gradient of the Unload/Reload Line
λ	Rate effect per log cycle
$\lambda_{\varepsilon q=1\%}$	Rate effect per log cycle of strain rate at 1% shear strain
$\lambda_{\varepsilon q=10\%}$	Rate effect per log cycle of strain rate at 10% shear strain
λ_{max}	Maximum rate effect observed at any given shear strain
λ_{NCL}	Gradient of the normal consolidation line
$\lambda_{peak,pl}$	Rate effect per log cycle at the plastic limit (PL) (using peak strength rate effect definition)
λ_{pl}	Rate effect per log cycle at the plastic limit (PL) (using strain-based rate effect definition)
Γ	Intercept on the critical state line (CSL) at 1 kPa
Ψ_{ref}	Reference state parameter

1 Introduction

Viscous rate effects cause the undrained shear strength of fine-grained soils such as clays to increase with strain rate, with the increase normally expressed as the percentage increase in shear strength (compared to the shear strength at a selected reference strain rate) for every log cycle increase in strain rate (e.g. Kulhawy and Mayne [17]). Viscous rate effects are distinct from drainage-related time effects, although there can be interaction between these effects [33]. An accurate understanding of viscous rate effects is important for many geotechnical activities where high strain rates are induced, such as rapid load pile testing [6, 7], interpretation of offshore site investigation using techniques such as free-falling penetrometers [9, 10], offshore deep penetrating anchors (DPA) [22, 27], prediction of subsea cable plough resistance [32] and offshore helical pile installation [48]. Wahl et al. [42] also highlight that viscous rate effects are important in the modelling of lateral capacities of offshore monopiles as well as spudcan penetration resistance. Viscous rate effects are also key to the analysis of rapid geotechnical failures including landslides [21, 24, 28] and transmission tower uplift [30]. Regardless of whether the study of these problems is physical or numerical, accurate rate effect parameters are important for the correct analysis and prediction of the behaviour.

Rate effects are typically assumed to be a consistent value of 10% per log cycle increase in strain rate [17], but a number of studies have shown the variability of viscous rate effects with the reported values typically ranging from 5 to 20% per log cycle [26, 27, 43]. Even within the triaxial compression dataset used by Kulhawy and Mayne [17], further analysis [31] shows that individual clays exhibit rate effects ranging from 6% per log cycle (Vicksburg clay) up to 17% per log cycle (Lyndhurst clay). While such variations may appear small, many of the high strain rate activities described previously occur at strain rates several orders of magnitude higher than the strain rate at which conventional material characterisation is often carried out. Taking deep penetrating anchors as an example, even a difference of 5% per log cycle in the rate effect would lead to an error of up to 25% in the predicted shear strength of the soil [31].

Previous studies have indicated that several potential factors may influence and control the magnitude of rate effects, aside from the fact that rate effects clearly vary between different soils. The state of the soil (whether measured in terms of its moisture content, liquidity index or otherwise) has been shown to affect the rate effect [3, 4, 8], as well as the soil's stress history in terms of the overconsolidation ratio (OCR) [4]. However, these variables are closely interlinked, and further study is required to investigate whether the OCR is independently influencing the rate effect, or whether any change in the rate effect is purely related to changes in the state (i.e. moisture content) of the soil caused by swelling as the soil becomes overconsolidated. Rate effects have also been shown to vary with strain level [1], and different effects are seen depending on whether the small or large strain level range is considered [14, 23].

Numerous studies have shown that viscous rate effects increase with moisture content [3, 7, 8, 11]. These studies cover a wide range of soils and used methods ranging from free-falling penetrometers to triaxial testing, giving some confidence in the observation. However, there is a need for further research to conclusively identify the form of the

relationship between rate effects and moisture content/liquidity index, as well as to confirm which of these is the controlling parameter. The question of whether rate effects occur at or below the plastic limit has been investigated by both Brown and Hyde [7] (rapid load pile testing) and Stone and Phan [41] (motorised laboratory cone tests), and the former suggested no rate effects occur, while the latter suggested rate effects of around 10% per log cycle at the plastic limit. There is little other research published on this specific consideration.

The influence of stress history (OCR) has also been the subject of several studies, the majority of which suggest no clear influence of OCR on rate effects [7, 14, 19, 37, 49]. Those studies which do suggest a small increase in rate effect with OCR [4] have generally not accounted for the fact that tests conducted at higher OCRs typically have higher moisture contents than normally consolidated tests with the same level of preconsolidation (due to swelling during the overconsolidation process), which may explain the finding. This has also been considered by Brown and Hyde [7] based on rapid load pile testing (RLT), which suggested that it may be soil state (in terms of moisture content) rather than stress history (or OCR) that controls viscous rate effects.

Considering, the strain dependence of rate effects, the studies on this issue can be broadly split into those that have investigated small strain behaviour [23, 39, 40] and large strain behaviour [1, 2, 14]. In terms of studies focussing on small strain behaviour, there is a general consensus that no viscous rate effects are observed below the elastic strain threshold, and that after this point, rate effects increase with shear strain level [23]. Rate effects at very low shear strain rates (typically $< 0.01\%$/hr) may however be influenced by creep of the specimen during testing [18], where relaxation can lead to a reduction in the measured deviator stresses. In addition, the creep coefficient, $C_{\alpha e}$, is also often used to model rate dependent behaviour of soft clays, such as in elastic-viscoplastic constitutive models [46, 47]. The links between creep and viscous rate effects are not explored in this study. Rate effects at large strain levels have either been shown to show little change with increasing strain level [1] or to reduce with increasing strain level [2, 14]. Knowledge of how viscous rate effects vary with strain level is key to the analysis of many of the rate effect applications previously mentioned where a strain-based approach is required for interpretation. For example, using Statnamic pile testing, Powell and Brown [29] highlighted the need for accurate rate effect parameters across all strain levels, without which interpretation is challenging.

This paper aims to investigate undrained viscous rate effects using high-speed undrained triaxial testing, in order to determine the independent influences of soil state and stress history as well as rate effect variation with strain level. Viscous rate effects have been investigated by other methods such as shear vane testing [5, 44]; however, challenges in the determination of shear strain and drainage conditions in these approaches complicate their use when considering a strain level-based rate effects model. Rate effects related to time for drainage (i.e. rate effects in the partially drained range) have been previously considered by Robinson et al. [33] and will not be further investigated here. The consideration of variation with strain level here will focus particularly on the large strain range ($\varepsilon_q > 1\%$), which is the most appropriate range for the majority of geotechnical applications where high strain rates occur. The paper aims to develop correlations which allow the (large strain) rate effect per log cycle to be quantified for any soil state or strain level.

2 Methodology

The tests were carried out on reconstituted Speswhite Kaolin, the properties of which are shown in Table 1. Reconstituted samples were used as variability and imperfections in field samples can impact on the measured deviator stresses, influencing the measure viscous rate effects. The reconstitution process allowed careful control over sample quality, avoiding these issues. The samples were first prepared as slurry with a moisture content of 125% using de-aired, de-ionised water before being one dimensionally consolidated to a mean effective stress of 150 kPa for three days. These were then trimmed to 200 mm length and 104 mm diameter to create triaxial samples. Uniformity of the one dimensionally consolidated sample was assured by lubricating the consolidation tube with PTFE spray, and samples were taken from the central section to avoid the non-uniform ends. Once installed in the triaxial apparatus, the sample was saturated to an effective stress of 50 kPa at a back pressure of 250 kPa and then re-consolidated to the required effective stress for the test to induce isotropic initial conditions for 24–48 h as required (at a back pressure of 300 kPa). In overconsolidated tests, the sample was first consolidated to the maximum mean effective stress ($p'_{0,\max}$) before being allowed to swell for 24 h at the effective stress to be used in that test.

Sample drainage was facilitated by using vertically orientated filter paper drains (for radial drainage) on the surface of the sample, connected to both the top and bottom drainage valves. These were required as the use of oversized lubricated end platens in the testing meant that conventional vertical drainage was not possible, and the radial drainage had the additional benefit of significantly reducing consolidation times. Effectiveness of the filter paper drains

Table 1 Summary of material properties for the Kaolin tested

Property	Value	Method
Plastic Limit, PL (%)	32.5	Thread rolling method
Liquid Limit, LL (%)	65.0	BS fall cone
Plasticity Index, PI (%)	32.5	Calculated
Clay Fraction, CF (%)	82	BS hydrometer
Activity, A (%)	39.6	Calculated
Proportion of Kaolinite (%)	80	X-ray diffraction and Rietveld analysis
Proportion of Illite (%)	18	
Proportion of Quartz (%)	2	
Specific Surface Area, SSA (m^2/g)	36.7	Methylene blue absorption (Following Santamarina et al., [36])
Permeability, k (m/s)*	0.76×10^{-9} to 1.17×10^{-9}	Permeability tests (constant pressure difference) on 38 mm triaxial samples (without filter drains) in a triaxial cell subject to the same consolidation conditions as the 100-mm samples in this paper
Coefficient of Consolidation, c_v (m^2/year)*	23.5–48.1	Calculated using k (see above) and m_v (compressibility) from 38 mm triaxial tests subject to the same consolidation conditions as the 100-mm samples in this paper
NCL Gradient, λ_{NCL}	0.168	38 mm triaxial tests ($\dot{\varepsilon}$ = 1%/hr, isotropic)
Unload/Reload Line Gradient, κ	0.021	
NCL Intercept, N	3.101	
CSL Intercept, Γ	2.988	
Gradient of CSL in q-p' space, M	0.851	
Reference State Parameter, Ψ_{ref}#	0.113	

*Effective stress ranging from 300 to 1000 kPa, using a 100 kPa stress increment

#For normally consolidated conditions

at higher mean effective stresses (p'_0 = 1000 kPa and above) was maintained by the use of a double layer of filter paper. Head and Epps [15] recommended that for 100-mm diameter samples, filter paper drains should cover no more than 50% of the sample surface area to ensure the reinforcing effect on the deviator stress is no more than 3 kPa. In this study, the filter paper drains covered 23% of the surface area, ensuring that the reinforcing effect is less than this value. Membrane corrections were also applied as recommended by Head and Epps [15].

The tests were carried out in a GDS advanced electromechanical dynamic triaxial rig (MiniDYN) specially modified to carry out high-speed monotonic tests. The setup of the triaxial system is shown in Fig. 1. The rig was capable of axial displacement rates of 100 mm/s, and during high-speed testing it was controlled by a GDS digital control system capable of controlling the axial displacement within a time interval of 0.1 ms (10,000 Hz). Both the back and cell pressures were provided by GDS pressure controllers. Lubricated end platens of a similar design to those proposed by Rowe and Barden [15, 34] were used to minimise the inhomogeneity caused by end restraint conditions [15, 38]. This arrangement consists of smooth, enlarged aluminium end platens (115 mm diameter) with a thin layer of silicone grease, upon which a circle of latex with radial slits is placed, minimising boundary effects which could lead to sample inhomogeneity. This is particularly important in high strain rate triaxial tests, where sample inhomogeneity can lead to the applied shear strain rate varying across the specimen. The system applied load to the triaxial specimen via the bottom platen, with global displacements measured by an encoder to a resolution of 1.3 μm. As part of the lower platen arrangement, a balanced ram system also ensured that the cell volume change during shearing was minimal even at the elevated shearing rates implemented [13]. Robinson [31] showed that with the balanced ram, even at the highest strain rate (100,000%/hr) the cell pressure deviated by no more than 2 kPa from the intended value. The axial force applied to the specimen was measured by a GDS Type 9 submersible load cell with a range of 5 kN and a measurement resolution of 0.5 N.

The system control and logging was provided by a GDS Dynamic Control System (GDS DCS) where details of the

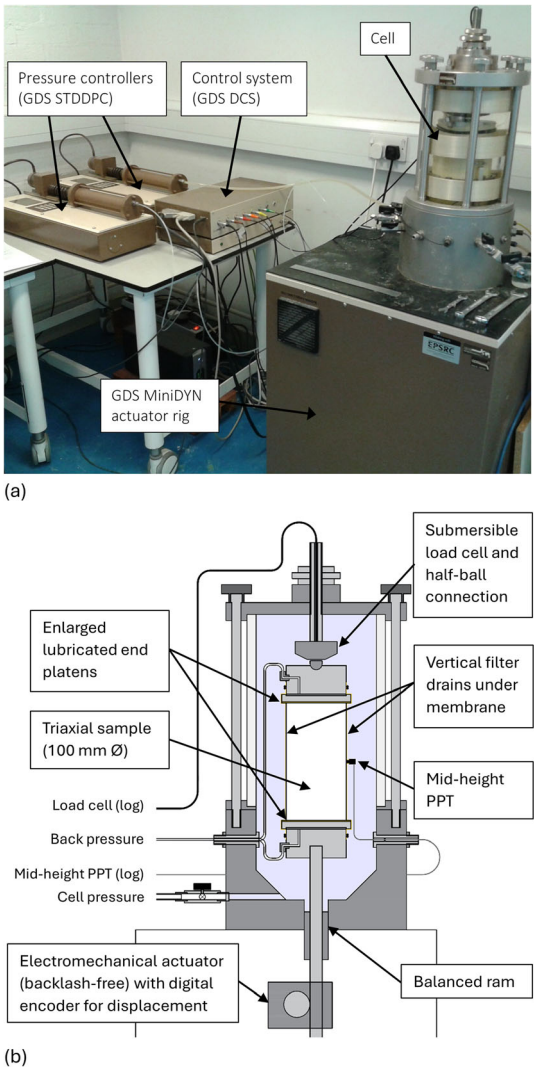

Fig. 1 **a** Photograph of the triaxial system setup and **b** schematic drawing of the triaxial cell, sample and instrumentation

required displacements for each test are transferred to the GDS DCS and the test is conducted using a PID control loop, with a common control and logging frequency of 10,000 Hz per channel. To avoid inertial effects and ensure accurate test control, at the beginning of the shearing stage, the acceleration of the base platen to the required test velocity was set at 1.90 m/s^2. This was achieved by modifying the requested displacement waveform to have a lead-in, which limited the effect of sample inertia on the deviator stress in the fastest test ($\dot{\varepsilon}$ = 100,000%/hr) to less than 0.7 kPa. At the end of the shearing stage (at approximately 20% shear strain), the system brought the base platen to a full stop at the motor's braking rate. Data were not logged during the braking phase. Further details on the testing apparatus and methodology can be found in Robinson [31].

The testing programme consisted of triaxial tests at axial strain rates from 300 to 180,000%/hr in order to investigate rate effects over as large a range as possible. These strain rates ensure that all tests exist within the undrained range as described by Robinson et al. [33], regardless of the externally imposed drainage conditions. These were carried out for normally consolidated samples at effective stresses ranging from 300 to 1350 kPa. The final consolidated sample dimensions (before the shearing stage) ranged from 196.9 mm (H) × 102.1 mm (Ø) for p'_0 = 300 kPa to 180.3 mm (H) × 98.6 mm (Ø) for p'_0 = 1350 kPa. Two overconsolidated samples were also prepared (OCR = 6, p'_0 = 108 kPa) and tested at the extremes of the strain rates only (see Table 2 for more detail on the testing programme). These tests were conducted in the same manner as the normally consolidated tests, with the exception of an additional swelling stage where the effective stress was reduced from p'_{max} = 650 kPa to p'_0 = 108 kPa.

3 Results and discussion

The main impacts of varying strain rates can be seen in Fig. 2a where each increase in strain rate is marked by an increase in peak deviator stress, when compared to other tests at the same initial mean effective stress. The peak deviator stress was defined as the point at which the maximum recorded deviator stress occurred in that test [33]. A shift in the strain level at which peak deviator stress occurs is also observable with this strain level appearing to reduce with increasing strain rate, indicating that rate effects may vary with strain level and are not constant throughout the test [33]. Beyond 12% axial strain, the specimens were observed to localise as a shear plane formed, with the strain at which this occurred varying significantly (at strains ranging from 12 to 20%). There was no clear trend in the strain level at localisation in relation to strain rate. Peak deviator stress was reached well before the localisation occurred in all cases. The data from Fig. 2a are also shown normalised by the initial mean effective stress, p'_0, in Fig. 2b. Photographs of a typical normally consolidated Kaolin sample, before and after testing, are shown in Fig. 3a and b, respectively. In the photograph after testing, the membrane and filter drains have been removed to show the localisation. Direct observation of the sample (at $\dot{\varepsilon}$ = 1000 and 10,000%/hr, where the test duration was sufficiently long to allow this) during testing indicated that this localisation began at the same strain level at which the effects of the localisation appeared in Fig. 2a ($\varepsilon_q > 12\%$).

Figure 4 shows the peak deviator stresses extracted from the stress–strain behaviour in Fig. 2a for each strain rate. Comparison of the data suggest that the rate dependent increase in deviator stress was best modelled using a semi-log relationship of the form in Eq. (1) and as proposed by Sheahan et al. [37]. In the equations shown in Fig. 4, the

Table 2 Programme of large strain CIU tests conducted on Kaolin specimens

Test designation	Mean effective stress, p'_0 (kPa)	Axial strain rate, $\dot{\varepsilon}$ (%/hr)	OCR	Liquidity index, LI
KLN-TU-L1	300	1000	1	0.32
KLN-TU-L2	300	10,000	1	0.32
KLN-TU-L3	300	100,000	1	0.32
KLN-TU-L4	650	1000	1	0.18
KLN-TU-L5	650	10,000	1	0.18
KLN-TU-L6	650	100,000	1	0.18
KLN-TU-L7	1000	1000	1	0.10
KLN-TU-L8	1000	10,000	1	0.10
KLN-TU-L9	1000	100,000	1	0.10
KLN-TU-L10	1350	1000	1	0.02
KLN-TU-L11	1350	10,000	1	0.02
KLN-TU-L12	1350	100,000	1	0.02
KLN-TU-L13	108 (p'_{max} = 650 kPa)	300	6	0.22
KLN-TU-L14	108 (p'_{max} = 650 kPa)	180,000	6	0.22

Due to the use of large 100-mm diameter samples, repeat tests were not conducted

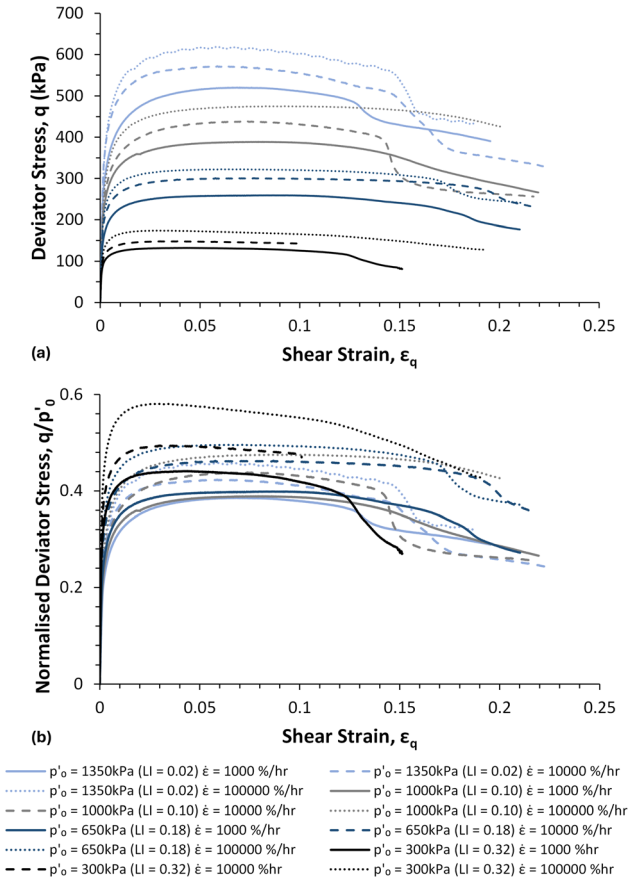

Fig. 2 **a** Variation of deviator stress with shear strain at different initial mean effective stresses showing the influence of axial strain rate (normally consolidated conditions) and **b** normalised by the initial mean effective stress

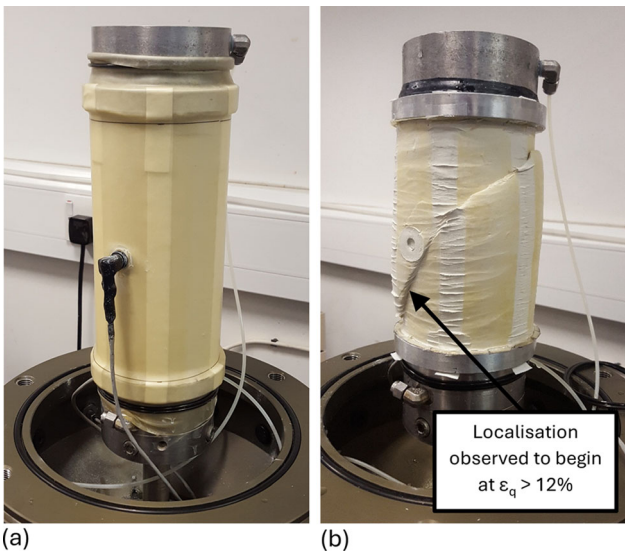

Fig. 3 Photographs of a typical normally consolidated Kaolin triaxial sample **a** before and **b** after high-speed triaxial testing

values for the coefficient represent the absolute increase in deviator stress (in kPa) per log cycle increase in strain rate and the constant represents the intercept at a shear strain rate of 1%/hr (the base of a semi-log relationship). As shown, the absolute increase in peak deviator stress per log cycle is greater at higher effective stresses, ranging from 20.8 kPa/log cycle at p'_0 = 300 kPa to 50.9 kPa/log cycle at p'_0 = 1350 kPa. However, when deriving λ (Eq. 1), this is based not on effective stress but on the ratio of the peak deviator stresses (normalised) [33].

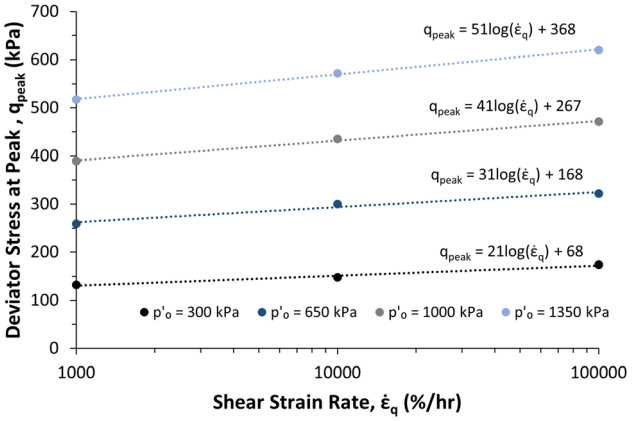

Fig. 4 Variation of peak deviator stress with shear strain rate for CIU specimens prepared at initial mean effective stresses ranging from p'_0 = 300 to 1350 kPa

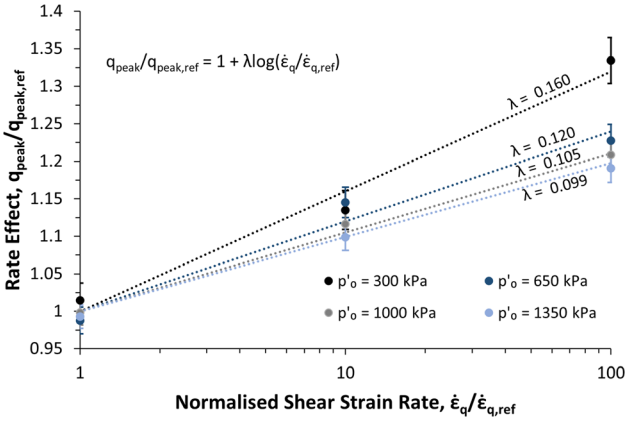

Fig. 5 Determination of normalised rate effects at peak strength for normally consolidated Kaolin at mean effective stresses from 300 to 1350 kPa ($\dot{\varepsilon}_{q,ref}$ = 1000%/hr) with error bars showing the propagation errors based on measurement uncertainties

$$\frac{q}{q_{\text{ref}}} = 1 + \lambda \log\left(\frac{\dot{\varepsilon}}{\dot{\varepsilon}_{\text{ref}}}\right) \tag{1}$$

where λ is the increase in q/q_{ref} per log cycle, q is the deviator stress, and q_{ref} is the peak deviator stress determined at the reference strain rate which marks the transition from partially drained behaviour to undrained drained behaviour which was determined in a previous study for Kaolin and described in detail in Robinson et al. [33]. Robinson et al. [33] suggested that this transition for Kaolin occurred at axial strain rates of between 132 and 220%/hr (normalised velocity, V = 3.1 to 8.2 as defined in Eq. 2) for 100-mm triaxial specimens, depending on the effective stress used in the test.

$$V = \frac{vd}{c_v} \tag{2}$$

where v is the axial velocity, d is the characteristic length related to drainage, and c_v is the coefficient of consolidation. For consistency, a reference axial strain rate of 1000%/hr has been adopted to ensure no local drainage can occur within the specimens during testing. A more detailed discussion of reference rate selection in rate effect studies can be found in Robinson et al. [33] and Robinson [31].

The normalised rate effect per log cycle shown in Fig. 5 was determined by normalising the peak deviator stresses by the peak deviator stress at a shear strain rate of 1000%/hr, q_{ref} (for the same corresponding initial mean effective stress). Vertical error bars are also shown in Fig. 5 for information, indicating the calculated propagation errors based on the uncertainties in the measurements that contribute to the data shown. These include load cell calibration accuracy and resolution, as well as the impact of pressure controller calibration accuracy and resolution on the deviator stress. The horizontal axis has also been normalised by the lowest shear strain rate of 1000%/hr, such that the lowest normalised strain rate will be 1; the intercept of the semi-logarithmic relationship. Figure 5 shows the values of λ ranging from 0.160 (16% per log cycle) at the lowest effective stress down to 0.099 (9.9% per log cycle) at the highest effective stress of p'_0 = 1350 kPa (close to the plastic limit, LI = 0.02, Table 2), which is within the typical range for λ of 0.1 to 0.2 suggested by Einav and Randolph [12] and Sheahan et al. [37]. This reduction in λ with increasing effective stress (or reducing moisture content) is consistent with several previous studies [3, 4, 8]. However, it should be noted that these former studies have provided little insight into the form of the relationship between moisture content and rate effects.

Figure 6 shows the variation of λ determined from Fig. 5 with liquidity index (See Eq. 3) rather than effective stress. The rate effect per log cycle at peak deviator strength has been denoted λ_{peak}. Other previous studies [3, 8, 41] indicate that there is little variation in the rate effect below the plastic limit, making this a useful

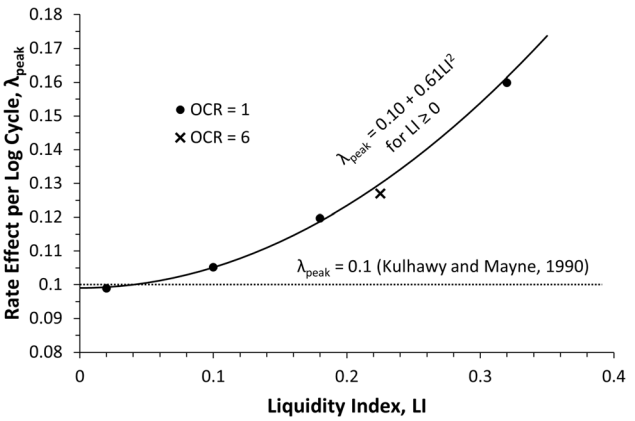

Fig. 6 Variation of rate effect at peak strength with liquidity index for normally consolidated and overconsolidated Kaolin

reference point. This suggests that a correlation with liquidity index (rather than moisture content or specific volume) may be appropriate for viscous rate effects, as the plastic limit is suggested by these previous studies as a transition point below which the viscous rate effect is relatively insensitive to changes in moisture content. The data from this study supports this assumption, with the change in λ_{peak} reducing as the plastic limit is approached, reaching a value of 9.9% at a liquidity index of 0.02. It was found that the data could be modelled using an equation of the form shown in Eq. (3) such that λ_{peak} varies with the square of liquidity index in the range $0 < LI < 0.4$.

$$\lambda_{peak} = \lambda_{peak,PL} + \alpha_{peak} LI^2 \quad (3)$$

where $\lambda_{peak,PL}$ is the rate effect per log cycle based upon on peak deviator stress determined at the plastic limit, α_{peak} is a coefficient and LI is the liquidity index. The coefficient, α_{peak}, accounts for the dependence of viscous rate effects (λ_{peak}) on soil state (in terms of LI) for a particular soil. As α_{peak} will have a unique value for any given soil (i.e. is a material constant), there is a need for further research to identify which easily characterisable soil material properties can be correlated with α_{peak} to allow estimation of viscous rate effects for different soils. It is recommended that future rate effect studies should determine α_{peak} for the soil being investigated, and publish this so that a database of these values can be compiled.

3.1 Comparison with previous studies and the effect of overconsolidation ratio

For normally consolidated kaolin, $\lambda_{peak,PL}$ and α_{peak} were found to be 0.10 and 0.61, respectively. Kulhawy and Mayne [17] suggests a constant value of λ_{peak} of 0.1. Liquidity index data for the tests analysed is not presented, however, and many of the field samples were overconsolidated and likely to be closer to the plastic limit, skewing the data towards the lower range of rate effects and explaining why rate effects are often quoted as being 10% per log cycle. The suggested value of 0.1 compares well to the rate effect determined near the plastic limit in this study. Given that clays analysed by Kulhawy and Mayne [17], such as Lyndhurst clay, exhibited rate effects of up to 17% per log cycle, the rate effect observed at the highest liquidity index tested of 16% per log cycle shown in Fig. 6 appears consistent with previous studies.

Figure 7 shows the rate effects from Bea [3] and Chow and Airey [8] against liquidity index. Bea [3] carried out triaxial tests on Gulf of Mexico Clay (GMC) and Chow and Airey [8] used Free Falling Penetrometer (FFP) tests in Kaolin (with substantially different properties to that used in this study). However, it is still useful to validate the form of the proposed relationship to confirm if it is able to model

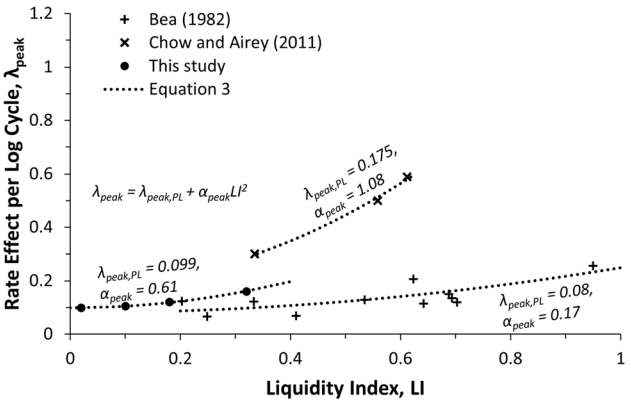

Fig. 7 Comparison of proposed relationship with rate effects at peak from other studies

the derived rate effects, despite the fact that the magnitude of the rate effects may vary for different soils [31]. While other studies have investigated viscous rate effects, in many of these studies, insufficient data are presented in terms of moisture content and Atterberg limits to allow comparison with the data presented here, which considers the influence of soil state. The value of $\lambda_{peak,pl}$ of 0.08 derived from the data from Bea [3] supports the idea that near the plastic limit, rate effects are more likely to be close to the value of $\lambda = 0.1$ suggested by Kulhawy and Mayne [17]. This is not the case for the Chow and Airey [8] data but it is noted that testing was not undertaken at low moisture contents in that study, which causes uncertainty in the estimation of $\lambda_{peak,pl}$ for Chow and Airey [8]. The Free Falling Penetrometer tests in Chow and Airey [8] also have the additional challenge of separating inertia and drag effects from the viscous response.

While it was previously noted that the rate effect correlation proposed for Kaolin (Eq. 3) is valid for the range of $0 < LI < 0.4$, Fig. 7 does give confidence that the general LI^2 form of the relationship may potentially be valid at greater liquidity indexes up to LI = 1. In each of the studies shown, the LI^2 relationship is shown to fit the data well with the variation in viscous rate effects becoming relatively insensitive to changes in moisture content as the plastic limit is approached.

Evidence of the influence of overconsolidation ratio on rate effects is variable. Examples include Briaud and Garland [4] who found that rate effects increased with overconsolidation ratio (OCR), while Sheahan et al. [37], Lehane et al. [20] and Graham et al. [14] found no impact of OCR. To consider this issue further, additional tests on Kaolin specimens at an OCR of 6 (p'_{max} = 650 kPa, p'_0 = 108 kPa) were conducted (see Fig. 6). The rate effect per log cycle, λ, was found to be 0.127 for an OCR of 6 [31] which is slightly greater than the rate effect observed at the same preconsolidation pressure in normally

consolidated Kaolin ($\lambda = 0.12$ for $p'_0 = 650$ kPa). However, when compared at the same liquidity index (i.e. similar specific volume or moisture content), it is clear that the overconsolidated testing fits well with the previously determined relationship between λ and *LI* from normally consolidated testing (See Fig. 6). With the limited testing undertaken here it would suggest that the soil state has a greater control on the viscous rate effects, and there is no additional effect over and above this of stress history. Further testing of overconsolidated samples would however be required to confirm this.

3.2 Strain level dependency

Up to this point, the viscous rate effects have been defined in terms of peak deviator stress but this affects the consistency of the calculated viscous rate effects when investigating strain level dependency, as the rate of testing was also seen to reduce the strain level at which peak deviator stress occurred (Fig. 8).

Figure 9 shows the strain at peak, normalised by the corresponding strain at peak at the reference strain rate, $\varepsilon_{q,\text{peak,ref}}$, of 1000%/hr. A clear trend can be seen in the normalised strain at peak which reduces linearly by approximately 12% per log cycle increase in strain rate. The relationship between strain at peak and shear strain rate for Kaolin was found to be as shown in Eq. (4).

$$\frac{\varepsilon_{q,\text{peak}}}{\varepsilon_{q,\text{peak,ref}}} = 1 - 0.12 \log\left(\frac{\dot{\varepsilon}_q}{\dot{\varepsilon}_{q,\text{ref}}}\right) \tag{4}$$

Sheahan et al. [37] considered the impact on strain level at peak deviator stress using triaxial testing of Boston Blue Clay (BBC). The strain levels at peak from that study are also shown in Fig. 9, although it should be noted that the data from Sheahan et al. [37] is from testing at substantially lower axial strain rates (0.05–50%/hr) and on a different

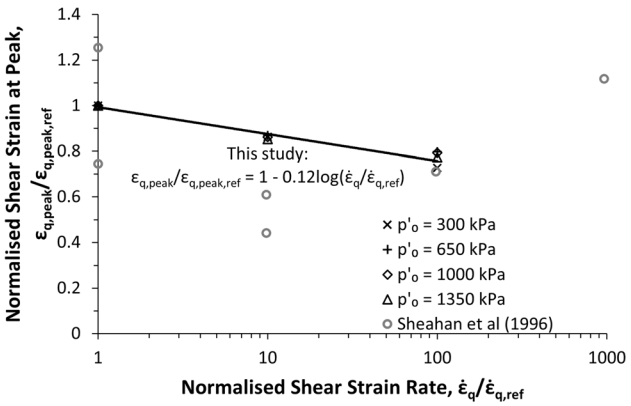

Fig. 9 Variation of normalised strain at peak with normalised shear strain rate from this study (Kaolin) compared with Sheahan et al. (1996) for Boston Blue Clay

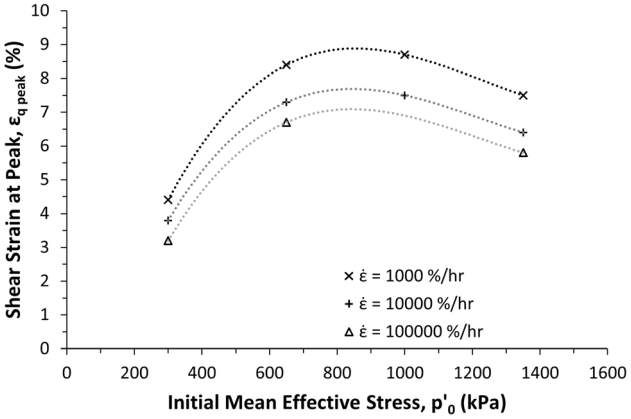

Fig. 8 Variation in shear strain at peak strength with effective stress for varying axial strain rates in Kaolin

clay. Nevertheless, the data from Sheahan et al. [37] highlights that there is a general reduction in $\varepsilon_{q,\text{peak}}$ with increasing strain rate (although there is significant scatter in that data).

The effect of rate of strain on the position of peak deviator stress (strain level) highlights the strain level dependent nature of rate effects i.e. depending on the strain level the rate effect may vary as suggested by Robinson et al. [33] and Graham et al. [14]. Figure 10 shows the stress–strain response of the specimens tested at each of the four initial mean effective stresses, annotated with the yield points, (defined as the elastic shear strain threshold, $\varepsilon_{q,EL}$) and observed initial shear secant moduli based on the global displacement measurements in a similar manner to Shibuya et al. [39]. From this, it can be seen that the yield point at the reference strain rate (at each of the effective stresses) marks a clear transition point above which rate effects begin to mobilise, as also found by Shibuya et al. [39] and Lo Presti et al. [23]. Below this yield point, negligible variation can be seen between the stress–strain curves at the various strain rates. Several previous studies have also reported the rate independence of deviator stress below the yield point [25, 35]. It is only beyond this point that strain rate dependent differences in the deviator stresses start to be seen (in large strain measurements). The slight crossover of the stress–strain curves in Fig. 10d at low strain levels is due to a small imperfection in the grease layer of one of the lubricated end platens specifically in test KLN-TU-L11 ($p'_0 = 1350$ kPa, $\dot{\varepsilon}_q = 10{,}000\%$/hr), which resulted in a small increase in the initial stiffness. The issue corrected itself by 0.5% shear strain during that test as the grease redistributed during shearing. No other tests were affected by this.

Figure 11 shows how the rate effects vary throughout the strain range (using a strain level-based definition of rate effects rather than rate effect at peak, as described in

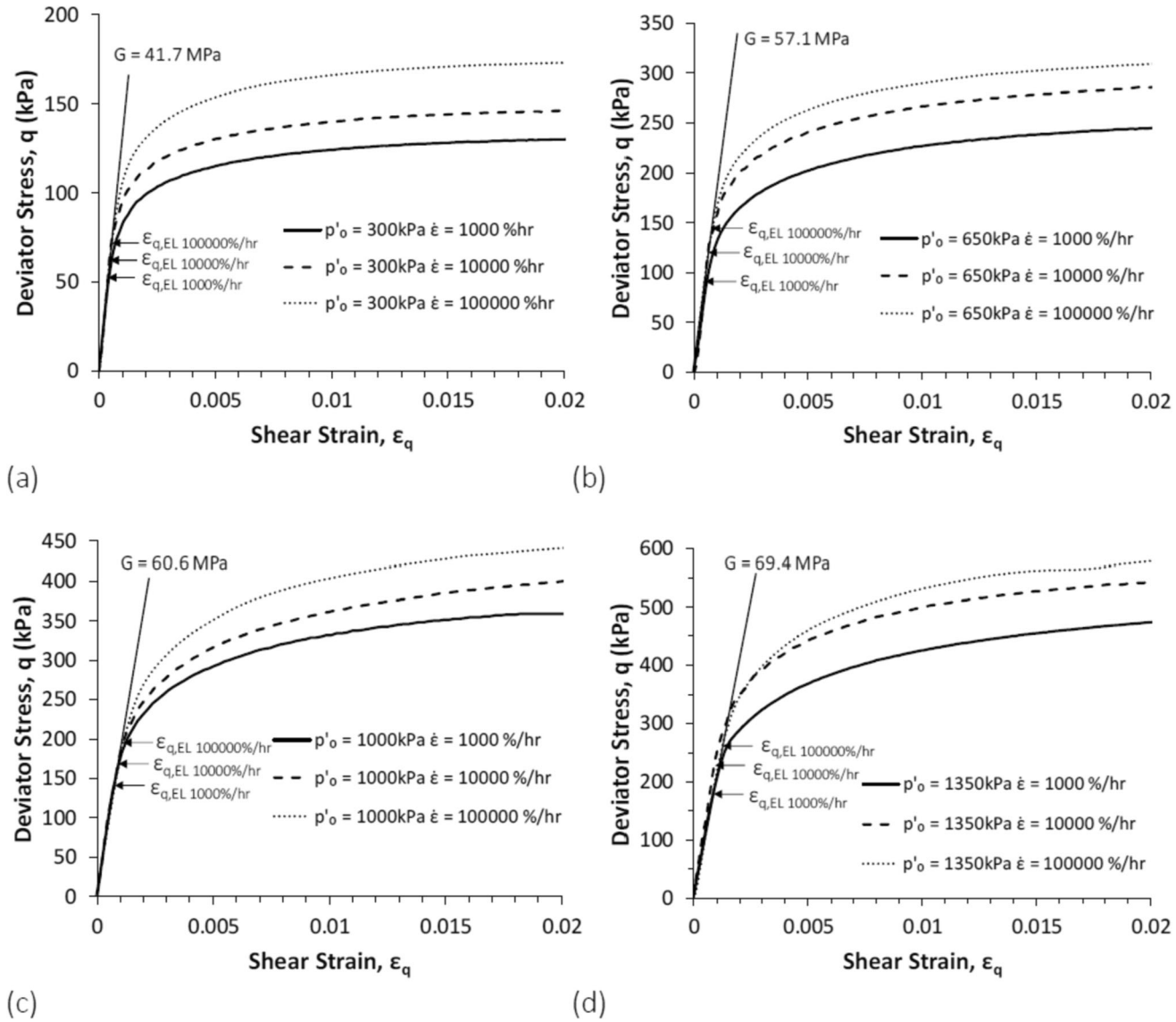

Fig. 10 Effect of axial strain rate on the stress–strain response of Kaolin from global strain measurements at **a** p'_0 = 300 kPa, **b** 650 kPa, **c** 1000 kPa and **d** 1350 kPa

Robinson et al. [33]). This approach calculates the rate effect at each increment of shear strain, rather than by calculating a single value using the peak deviator stress. This was achieved by extracting the deviator stress for each shear strain level shown from the tests at the three shear strain rates. At each specific strain level, a semi-log best fit was applied to determine the increase in deviator stress per log cycle increase in strain rate, which was then normalised by the deviator stress at that shear strain level from the reference strain rate test ($\dot{\varepsilon}_q$ = 1000%/hr) to give the values of λ shown in Fig. 11. This process was repeated for each of the effective stresses shown.

After rate effects begin to be mobilised following the yield of the specimen at the reference strain rate, the rate effects reach a maximum value, denoted λ_{max}, before beginning to degrade. The shear strain at which λ_{max} occurs has been denoted $\varepsilon_{q,\lambda max}$. This degradation continues until a strain of between 8 and 10% is reached, at which point the rate effect deviates from the preceding trend due to sample localisation and the beginning of visible shear plane formation. Data after this strain level are not shown, as after localisation the deformation of the sample occurs primarily on the shear plane. This means that the calculated shear strains and deviator stresses would no longer reflect the overall triaxial sample. For any group of three tests, there was no observable trend in the strain where localisation occurs with strain rate. Figure 11 also highlights the influence of soil state (influenced by p'_0) on rate effects throughout the strain range, not just at peak strength, as

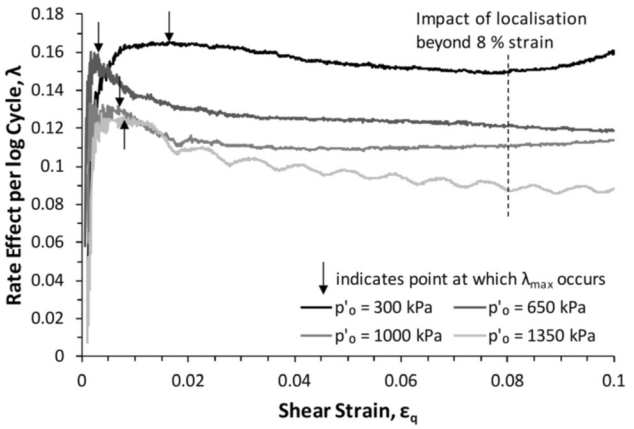

Fig. 11 Variation in rate effect with strain by defining λ using strain level rather than at peak strength (for $\dot{\varepsilon}_q$ = 1000–100,000%/hr)

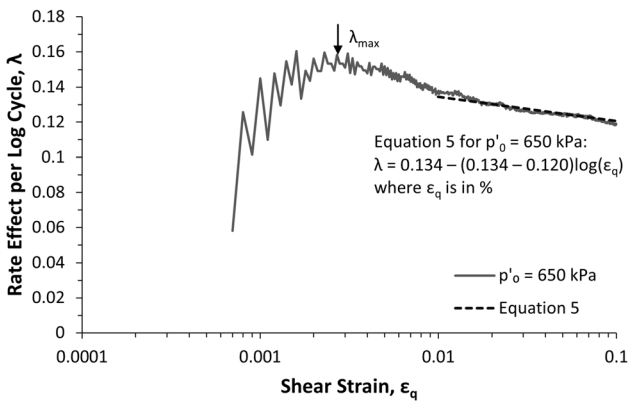

Fig. 12 Form of rate effect degradation after maximum rate effect at p'_0 in Kaolin (determined across $\dot{\varepsilon}$ = 1000–100,000%/hr) also showing an example fitting of Eq. (5) to the data

tests at lower effective stresses (and hence higher moisture contents) show larger rate effects across all strain levels.

Table 3 shows the shear strains at which the maximum rate effects were observed. These varied from 0.33 to 1.78%. On average, the shear strain at which the maximum rate effect occurred was 0.92%. There is some evidence that this value for the shear strain at λ_{max} of approximately 1% is relatively constant for different soils based on Lo Presti et al. [23] and Akai et al. [1]. Lo Presti et al. [23] found that the maximum strain rate coefficient, α, determined from resonant column testing was shown to occur near ε_q = 1% for a wide range of clays with plasticity indexes ranging from 10 to 40%.

In order for the variation of rate effects at large strains to be modelled, it is necessary to capture how rate effects degrade beyond the point of maximum rate effect, λ_{max}. Figure 12 shows a typical variation of λ with ε_q, plotted semi-logarithmically, which shows that beyond $\varepsilon_{q,\lambda max}$ rate effects appear to degrade linearly with $log(\varepsilon_q)$. This behaviour has been previously observed in studies including Graham et al. [14]. Considering all of the effective stresses investigated, a linear degradation of λ with $log(\varepsilon_q)$ was found to provide the best overall fit to the measured data.

The two key parameters in defining a semi-logarithmic relationship are the value at the intercept with the y-axis (at a value of 1 on the x-axis) and the change per log cycle. In this case, these correspond to the value of the rate effect at ε_q = 1%, which is the approximate location of the maximum rate effect, λ_{max}, and the change from this point to ε_q = 10%, which is typically close to the final point before localisation occurs. This means that it may be possible to model the strain dependent degradation of rate effects in the strain range from 1 to 10% using Eq. (5). The two rate effect parameters which require to be determined have been denoted $\lambda_{\varepsilon q=1\%}$ and $\lambda_{\varepsilon q=10\%}$, respectively. This equation is intended for use only in the large strain range (from ε_q = 1 to 10%).

$$\lambda = \lambda_{\varepsilon q=1\%} - \left(\lambda_{\varepsilon q=1\%} - \lambda_{\varepsilon q=10\%}\right) log\left(\varepsilon_q\right) \quad (5)$$

where ε_q is a percentage.

Figure 13 shows the variation of rate effect defined at both ε_q = 1% and 10% with liquidity index in a similar manner to that used to show the variation of λ_{peak} in Fig. 6. Where localisations have affected the measured rate effects before ε_q = 10%, the final point before the onset of localisation has been used instead of ε_q = 10%. The relationship between λ_{peak} and LI determined previously is also included for comparison. The rate effects at 1% and 10% shear strain can be represented by Eqs. (6) and (7) in the range 0 < LI < 0.4. Substituting these into Eq. (5) shows that the rate effect in Kaolin (at large strains beyond 1% shear

Table 3 Strain at which maximum rate effect occurs for Kaolin (based on external strain measurements)

p'_0 (kPa)	300	650	1000	1350	Average
Strain at λ_{max}, $\varepsilon_{q,\lambda max}$ (%)	1.78	0.33	0.71	0.87	0.92

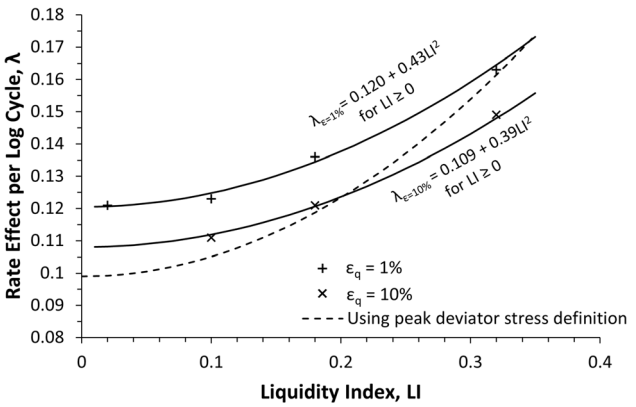

Fig. 13 Variation of rate effects at 1% and 10% shear strain with liquidity index in Kaolin

strain) at any liquidity index and strain level can be represented by Eq. (8).

$$\lambda_{\varepsilon q=1\%} = 0.120 + 0.43LI^2 \quad (6)$$

$$\lambda_{\varepsilon q=10\%} = 0.109 + 0.39LI^2 \quad (7)$$

$$\lambda = 0.120 + 0.43LI^2 - \left(0.011 + 0.04LI^2\right) log(\varepsilon_q) \quad (8)$$

where the constant (first term in the equation) represents the value at the plastic limit, λ_{pl}, which is the intercept with the y-axis at $LI = 0$, the coefficient represents the material-specific soil state effect parameter, α, and ε_q is in per cent.

Figure 14 presents a comparison of the values predicted by the proposed rate effect model (Eq. 8) with the measured data previously presented. This shows that, for the tests ranging from p'_0 = 300 to 1000 kPa, the model captures the measured rate effects well, with no rate effect varying from the model by more than ± 0.008 (± 0.8%). As can be seen in Fig. 14, there is some variation between the rate effects measured in the test at p'_0 = 1350 kPa and that predicted by the model due to control issues in this particular test, which has been omitted in the fitting shown in Fig. 15.

The coefficients in the equations shown in Fig. 14 represent the reduction in rate effect per log cycle of strain, $\Delta\lambda_{log(\varepsilon q)}$. By normalising these reductions by the corresponding value of the maximum rate effect ($\lambda_{\varepsilon q=1\%}$), the proportional change in the rate effect per log cycle of strain can be found. Figure 15 shows that this normalised change is near constant across all of the liquidity indices tested at -10% of the maximum rate effect per log cycle strain (i.e. apparently state independent). Using this, Eq. (8) can be simplified to Eq. (9), which it is proposed is valid for $0 < \text{LI} < 0.4$.

$$\lambda = \left(0.120 + 0.43LI^2\right) \times \left(1 - 0.10log\left(\varepsilon_q\right)\right) \quad (9)$$

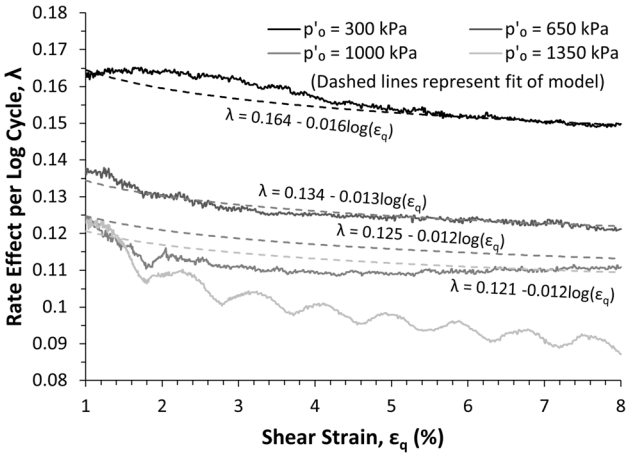

Fig. 14 Fit of proposed model to measured rate effects in Kaolin in normally consolidated conditions (determined over $\dot{\varepsilon}_q$ = 1000–100,000%/hr)

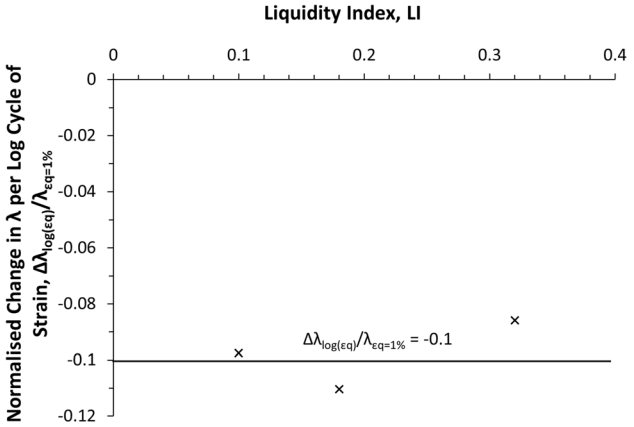

Fig. 15 Normalised degradation in rate effect per log cycle of strain post λ_{max}

where ε_q is in per cent.

Equation 9 (or Eq. 8) is particularly useful, as it allows the rate effect per log cycle to be estimated for Kaolin at any stage in a geotechnical activity, accounting for the combined effects of soil state (in terms of liquidity index) and strain level (for $1\% < \varepsilon_q < 10\%$). This could, for example, be used either in analytical solutions, or to facilitate the real-time updating of rate effects/shear strength in finite element (FE) analysis (e.g. as implemented in LDFE (Large Deformation Finite Element) analysis incorporating rate effects in a helical pile installation study by Zhou et al. [48]).

It is also useful to express the findings in terms of the undrained shear strength, c_u, which is commonly used in many analytical methods and soil models, but which is strain rate dependent. Using the equations presented earlier in the paper, for Kaolin, c_u can be expressed as a function of strain rate, $\dot{\varepsilon}$, liquidity index (via the rate effect parameter, λ) and the reference undrained shear strength, $c_{u,ref}$, at the reference strain rate, $\dot{\varepsilon}_{\text{ref}}$, as shown in Eq. (10).

$$\frac{c_u}{c_{u,\text{ref}}} = 1 + \lambda \log\left(\frac{\dot{\varepsilon}}{\dot{\varepsilon}_{\text{ref}}}\right) \quad (10)$$

where λ can be estimated based on liquidity index from Eq. (3) using $\lambda_{\text{peak,pl}} = 0.10$ and $\alpha_{\text{peak}} = 0.61$ for the Kaolin used here. $c_{u,\text{ref}}$ may be determined directly from soil tests conducted at a known value of $\dot{\varepsilon}_{\text{ref}}$, or alternatively it can be estimated using the correlation with liquidity index shown in Eq. (11) (Wroth and Wood, [45]; Knappett and Craig, [16]) such that both $c_{u,\text{ref}}$ and λ are dependent solely on LI. In this case, a value of $\dot{\varepsilon}_{\text{ref}}$ = 1%/hr would be suitable. It should, however, be noted that as c_u is typically defined at peak strength (i.e. not strain dependent), this method does not account for the strain dependence of rate effects previously discussed.

$$c_{u,\text{ref}} = 1.7 \times 10^{2(1-LI)} (\text{in kPa}) \quad (11)$$

The work described in this paper presents an opportunity for improving the accuracy of the estimation of rate effect impacts in a wide range of geotechnical activities. However, further research is required to expand the model in Eq. (9) to incorporate any rate effect behaviour at small strains (to provide a complete model that covers all strain levels), as well as to develop methods for predicting the coefficients and constants in Eq. (9) for different clays using easily available soil characterisation, which will be the focus of future papers and research. To expand the applicability of this work, there is also need for further research to determine whether sample anisotropy influences viscous rate effects, account for the differences in measured rate effects between reconstituted and natural samples, as well as to develop methods for correcting for the differences in viscous rate effects found when using different test methods. Further studies should also be conducted to investigate the impact of overconsolidation ratio and confirm whether this has any influence on viscous rate effects.

4 Conclusions

High speed CIU triaxial testing on Kaolin at a range of different initial mean effective stresses, using axial strain rates ranging from 1000 to 100,000%/hr, has identified a number of key aspects of viscous rate effects:

- Viscous undrained strain rate effects on peak strength in Kaolin were found to range from 10 to 16% per log cycle increase in strain rate (λ_{peak} = 0.10 to 0.16) at p'_0 = 1350 kPa and 300 kPa respectively which is greater than the commonly adopted 10% per log cycle.
- Viscous rate effects have been shown to be dependent on the soil state and this relationship can be described by a correlation between the rate effect per log cycle at peak strength, λ_{peak}, and the liquidity index, LI, of the soil tested (Eq. 3).
- The variation in viscous rate effects becomes relatively insensitive to changes in moisture content as the plastic limit is approached.
- Limited investigation of overconsolidation ratio showed it was found to have no observable influence on the magnitude of rate effects at peak strength, other than small increases which appeared to be due to changes in moisture content caused by swelling, and which are already described by the correlation with liquidity index.
- The strain at which peak deviator stress occurs is dependent on the strain rate.
- To accurately model rate effects, it is important to compare rate effects using a strain-based definition. Rate effects have been found to be strain dependent with the maximum rate effect, λ_{max}, occurring at around ε_q = 0.01 based on global strain measurements.
- The viscous rate effect at a strain, ε_q = 0.01, $\lambda_{\varepsilon q=1\%}$, can also be modelled using a correlation with liquidity index (Eq. 6).
- Above ε_q = 0.01 rate effects were found to reduce with $\log(\varepsilon_q)$, such that for every order of magnitude increase in applied strain, the rate effect λ reduced by 10% for Kaolin.
- The results of triaxial element testing at elevated rates are consistent with the findings of others and show similar strain dependant rate effects to those derived from rapid load testing.
- The viscous rate effect for Kaolin at shear strains greater than 1% can be calculated using a correlation with both liquidity index and shear strain (Eq. 9) which accounts for the combined effects of soil state (liquidity index) and strain level, allowing more accurate prediction of the impacts of rate effects in geotechnical activities.

In summary, this paper has investigated the influence of soil state on viscous rate effects at peak strength and proposed a correlation with liquidity index to model these in Kaolin. In particular, the plastic limit was shown to be a key point below which rate effects become insensitive to changes in moisture content, and the impact of OCR on rate effects was found to be negligible, although testing for the latter was limited. A strain-based model was also proposed to allow the viscous rate effects in Kaolin to be estimated at any liquidity index ($0 < LI < 0.4$) and strain level ($1\% < \varepsilon_q < 10\%$). Future work will investigate how this model can be expanded to incorporate other types of clays and to include small strain rate effect behaviour.

Acknowledgements This work is based on the corresponding author's PhD Thesis (Robinson, [31]) which was supported by funding from the University of Dundee Division of Civil Engineering and the Institution of Civil Engineers Research and Development Enabling Fund (Grant R&D1201), which is gratefully acknowledged.

Author contributions Scott Robinson performed conceptualisation, methodology, investigation, and writing—original draft. Michael Brown performed conceptualisation, methodology, writing—review and editing, supervision, and funding acquisition. Jonathan Knappett performed writing—review and editing and funding acquisition. Andrew Brennan performed writing—review and editing and funding acquisition. Diego Duran Caballero performed writing—review and editing. Marcos Arroyo performed writing—review and editing.

Data availability The data from the triaxial tests presented in this paper are available online via the University of Dundee's institutional repository and may be accessed at https://doi.org/10.15132/10000274.

Declarations

Conflict of interest The authors declare there are no competing interests.

References

1. Akai K, Adachi T, Ando N (1975) Existence of a unique stress-strain-time relation of clays. Soils Found 15(1):1–16
2. Balderas-Meca J (2004) Rate effects of rapid loading in clay soils. PhD Thesis, University of Sheffield, UK
3. Bea RG (1982) Soil strain rate effects on axial pile capacity. In: Proc. 2nd Int. Conf. on Numerical Methods in Offshore Eng., 107–132
4. Briaud J-L, Garland E (1985) Loading rate method for pile response in clay. J Geotech Eng ASCE 111(3):319–335
5. Biscontin G, Pestana JM (2001) Influence of peripheral velocity on vane shear strength of an artificial clay. Geotech Test J 24(4):423–429
6. Brown MJ (2008) Recommendations for Statnamic use and interpretation of piles installed in clay. Rapid load testing on piles. CRC Press, London, pp 23–36
7. Brown MJ, Hyde AFL (2008) Rate effects from pile shaft resistance measurements. Can Geotech J 45:425–431. https://doi.org/10.1139/T07-115
8. Chow SH, Airey DW (2011) Rate effects in free falling penetrometer tests. Proc. Int. Symp. on Deformation Characteristics of Geomaterials, Seoul, 1–3 September 2011.
9. Chow SH, O'Loughlin C, White D, Randolph M (2017) An extended interpretation of the free-fall piezocone test in clay. Géotechnique 67(12):1090–1103
10. Collico S, Arroyo M, Kopf A, Devincenzi M (2022) A probabilistic Bayesian methodology for the strain-rate correction of dynamic CPTu data. Can Geotech J 60(5):669–686
11. Diaz-Rodriguez JA, Martinez-Vasquez JJ (2005) Strain rate behavior of Mexico City soils. In: Proceedings of the 16th International Conference on Soil Mechanics and Geotechnical Engineering (16th ICSMGE), Osaka, Japan, 333–336.
12. Einav I, Randolph MF (2005) Combining upper bound and strain path methods for evaluating penetration resistance. Int J Numer Methods Eng 63(14):1991–2016
13. GDS Instruments (2024) Datasheet—GDS Triaxial Cell Range. Accessed 23/10/2024; Available at: https://www.gdsinstruments.com/__assets__/Products/00109/Triaxial-Cell-Datasheet.pdf
14. Graham J, Crooks JHA, Bell AL (1983) Time effects on the stress-strain behaviour of natural soft clays. Géotechnique 33(3):327–340
15. Head KH, Epps RJ (2011) Manual of soil laboratory testing—Volume II: permeability shear strength and compressibility tests. Whittles Publishing, Caithness
16. Knappett J, Craig RF (2019) Craig's soil mechanics, 9th edn. CRC Press, London
17. Kulhawy FH, Mayne PW (1990) Manual on estimating soil properties for foundation design. Report EL-6800, Electric Power Research Institute, Palo Alto, California, USA.
18. Le T, Standing J, Potts D (2024) Reassessing variations in the small-strain stiffness of London Clay. Géotechnique 74(4):383–397
19. Lefebvre G, LeBeouf D (1987) Rate effects and cyclic loading of sensitive clays. ASCE J Geotech Eng 113(5):475–489
20. Lehane BM, O'Loughlin CD, Gaudin C, Randolph MF (2009) Rate effects on penetrometer resistance in kaolin. Geotech 59(1):41–52
21. Liang T, Knappett JA, Leung AK, Bengough G (2020) Modelling the seismic performance of root-reinforced slopes using the finite-element method. Géotechnique 70(5):375–391. https://doi.org/10.1680/jgeot.17.P.128
22. Lieng JT, Sturm H, Hasselø KK (2022) Dynamically installed anchors for floating offshore wind turbines. Ocean Eng 266(2022):1–2. https://doi.org/10.1016/j.oceaneng.2022.112789
23. Lo Presti DCF, Jamiolkowski M, Pallara O, Cavallaro A (1996) Rate and creep effect on the stiffness of soils. Measuring and Modelling Time Dependent Soil Behaviour, ASCE, 166–180
24. Meijer G, Bengough G, Knappett J, Loades K, Nicoll B (2019) Measuring the strength of root-reinforced soil on steep natural slopes using the corkscrew extraction method. Forests 10(12):1–19. https://doi.org/10.3390/f10121135
25. Mukabi JN, Tatsuoka F (1999) Influence of reconsolidation stress history and strain rate on the behaviour of kaolin over a wide range of strain. In: Proceedings of the 12th African Regional Conference: Geotechnics for Developing Africa, 365–377.
26. Nanda S, Sivakumar V, Hoyer P, Bradshaw A, Gavin KG, Gerkus H, Jalilvand S, Gilbert RB, Doherty P, Fanning J (2017) Effects of strain rates on the undrained shear strength of kaolin. Geotech Test J 40(6):951–962
27. O'Loughlin CD, Richardson MD, Randolph MF, Gaudin C (2013) Penetration of dynamically installed anchors in clay. Geotech 63(11):909–919
28. Pinedo PJ, Besenzon D, Mánica MÁ, Arroyo M, Gens A (2022) Exploring viscous effects on numerical simulations of static liquefaction triggering. In: Tailings2022: 8th international conference on tailings management, 131–138. Gecamin.
29. Powell JJM, Brown MJ (2006) Statnamic pile testing for foundation re-use. In: International conference on the re-use of foundations for urban Sites, Watford, UK, 19–20th October 2006, 223–236.
30. Rattley MJ, Richards DJ, Lehane BM (2008) Uplift performance of transmission tower foundations embedded in clay. ASCE J Geotech Geoenviron Eng 134(4):531–540. https://doi.org/10.1061/(ASCE)1090-0241(2008)134:4(531)
31. Robinson S (2019) Rate effect behaviour of different clays from high speed triaxial element testing. PhD Thesis, University of Dundee, Dundee, UK. Accessed 07/12/2021; Available at: https://discovery.dundee.ac.uk/en/studentTheses/rate-effect-behaviour-of-different-clays-from-high-speed-triaxial
32. Robinson S, Brown MJ, Matsui H, Brennan A, Augarde C, Coombs WM, Cortis M (2021) A cone penetration test (CPT) approach to cable plough performance prediction based upon centrifuge model testing. Can Geotech J 58(10):1466–1477. https://doi.org/10.1139/cgj-2020-0366
33. Robinson S, Brown MJ, Knappett J, Brennan A (2023) Impacts of reference strain rate and strain level dependency on rate effects in fine grained soils. Géotech Lett 13(1):48–53. https://doi.org/10.1680/jgele.22.00080
34. Rowe PW, Barden L (1964) Importance of free ends in triaxial testing. ASCE J Soil Mech Found Divis 90(SM1):1–27
35. Santagata, M. (2008) Effects of stress history on the stiffness of a soft clay. In: Proceedings of the 4th International Symposium on

Deformation Characteristics of Geomaterials, IS Atlanta '08, Atlanta, 95–123.
36. Santamarina JC, Klein KA, Wang YH, Prencke E (2002) Specific surface area: determination and relevance. Can Geotech J 39:233–241
37. Sheahan TC, Ladd CC, Germaine JT (1996) Rate-dependent undrained shear behaviour of saturated clay. J Geotech Eng ASCE 122(2):99–108
38. Sheng D, Westerberg H, Mattsson H, Axelsson K (1997) Effects of end restraint and strain rate in triaxial tests. Comput Geotech 21(3):163–182
39. Shibuya S, Mitachi T, Hosomi A, Hwang SC (1996) Strain rate effects on stress strain behaviour of clay as observed in monotonic and cyclic triaxial tests. Meas Model Time Dependent Soil Behav: ASCE GSP 61:214–227
40. Sorensen KK, Baudet BA, Simpson B (2010) Influence of strain rate and acceleration on the behaviour of reconstituted clays at small strains. Géotechnique 60(10):751–763
41. Stone KJL, Phan KD (1995) Cone penetration tests near the plastic limit. Géotechnique 45(1):155–158
42. Wahl MM, Hamre L, Eiksund GR, Tjelta TI, Suzuki P, Rose M (2023) Rate effects increasing lateral capacity of monopiles. In: Innovative Geotechnologies for Energy Transition—9th International SUT Offshore Site Investigation and Geotechnics Conference, London, UK, 12–14 September 2023, 1022–1030.
43. Whitman RV (1957) The behaviour of soils under transient loadings. In: Proceedings of the 4th International Conference on Soil Mechanics and Foundation Engineering (ICSMFE), **1**, 207–210.
44. Wilson LJ, Kouretzis GP, Pineda JA, Kelly RB (2016) On the determination of the undrained shear strength from vane shear testing in soft clays. In: Proceedings of the 5th International Conference on Geotechnical and Geophysical Site Characterisation (ISC5), Sydney, Australia, 455–460.
45. Wroth CP, Wood DM (1978) The correlation of index properties with some basic engineering properties of soils. Can Geotech J 15(2):137–145
46. Yin Z-Y, Xu Q, Yu C (2012) Elastic-viscoplastic modelling for natural soft clays considering nonlinear creep. ASCE Int J Geomech 15(5):1–10
47. Yin Z-Y, Jin Y-F, Shen S-L, Huang H-W (2017) An efficient optimization method for identifying parameters of soft structured clay by an enhanced genetic algorithm and elastic-viscoplastic model. Acta Geotech 12:849–867
48. Zhou S, Zhou M, Tian Y, Zhang X (2023) Effects of strain rate and strain softening on the installation of helical pile in soft clay. Ocean Eng 285(1):115370
49. Zhu J-G, Yin J-H (2000) Strain-rate-dependent stress-strain behaviour of overconsolidated Hong Kong marine clay. Can Geotech J 37:1272–1282